

# Veröffentlichung

Im Rahmen des SFB 880. [www.sfb880.tu-braunschweig.de](http://www.sfb880.tu-braunschweig.de)

## **Autoren**

Müller, Lars;Kozulovic, Dragan;Hepperle, Martin;Radespiel, Rolf

## **Titel**

Installation Effects of a Propeller Over a Wing with Internally Blown Flaps

## **Publisher o. Konferenz**

Proc. of the 30th AIAA Applied Aerodynamics Conference, No. AIAA 2012-3335, New Orleans, LA (USA)

## **Jahr**

2012

## **Internet-Link (Doi-Nr.)**

# Installation Effects of a Propeller Over a Wing with Internally Blown Flap

Lars Müller\* and Dragan Kožulović†

*Technische Universität Braunschweig, 38108 Braunschweig, Germany*

Martin Hepperle‡

*Deutsches Zentrum für Luft- und Raumfahrt, 38108 Braunschweig, Germany*

and

Rolf Radespiel§

*Technische Universität Braunschweig, 38108 Braunschweig, Germany*

Aiming at maximum climb performance, the lift-to-drag ratio and the installed thrust of a STOL transport aircraft can be enhanced through a synergistic propeller integration. Reynolds-Averaged-Navier-Stokes simulations have been conducted on a generic geometry to quantify the aerodynamic interactions between the propulsion system and a wing with blown flaps. At takeoff, a conventional tractor configuration shows a distinct thrust vectoring effect inducing large lift and drag increments. By relocating the propeller at midchord above the wing, the lift over drag ratio and the installed efficiency are considerably improved while losing half of the lift augmentation. Compared to a simple over-the-wing installation, a channel wing design with a partially embedded propeller has the advantage that the thrust vector is closer to the center of gravity resulting in a smaller pitching moment due to thrust. An issue of over-the-wing propellers is the inhomogeneous inflow to the propeller which leads to cyclic variations in blade load and reduced net thrust.

## Nomenclature

$b, s$	=	wing span, semispan of CFD geometry
$c_f$	=	skin friction coefficient
$c_l, c_d, c_m$	=	local airfoil lift, drag, pitching moment coefficients (CFD geometry)
$c_\mu$	=	jet blowing coefficient
$C_T$	=	thrust coefficient of one engine $C_T = \frac{T}{\rho_\infty \cdot D_p^4 \cdot n^2}$
$\hat{C}_T$	=	aircraft thrust coefficient $\hat{C}_T = \frac{2 \cdot T}{q_\infty \cdot S_{ref}}$
$d, h$	=	gap between propeller tip and wing surface, slot height
$D, C_D$	=	drag, drag coefficient of aircraft $C_D = \frac{D}{q_\infty \cdot S_{ref}}$
$D_P$	=	propeller diameter
$l, l_{MAC}$	=	chord length of CFD geometry, mean aerodynamic chord length of reference aircraft
$L, C_L$	=	lift, lift coefficient of aircraft $C_L = \frac{L}{q_\infty \cdot S_{ref}}$
Ma	=	Mach number
$M_y, C_{M,y}$	=	pitching moment, pitching moment coefficient of aircraft $C_{M,y} = \frac{M_y}{q_\infty \cdot S_{ref} \cdot l_{MAC}}$
$n$	=	shaft speed (revolutions per second)
$p, c_p$	=	static pressure, pressure coefficient
$P_S, C_{P,s}$	=	shaft power, shaft power coefficient $C_{P,s} = \frac{P_S}{\rho_\infty \cdot D_p^5 \cdot n^3}$

\*Research Assistant, Institute of Fluid Mechanics, Hermann-Blenk-Str. 37, 38108 Braunschweig, la.mueller@tu-bs.de.

†Professor, Institute of Fluid Mechanics, Hermann-Blenk-Str. 37, 38108 Braunschweig.

‡Research Engineer, Institute of Aerodynamics and Flow Technology, Lilienthalplatz 7, 38108 Braunschweig.

§Professor, Institute of Fluid Mechanics, Hermann-Blenk-Str. 37, 38108 Braunschweig, Senior Member AIAA.

$q$	=	dynamic pressure
$Re$	=	Reynolds number
$S, S_{ref}$	=	wing area of CFD geometry, wing area of reference aircraft
$T, t/t_{max}$	=	thrust of one engine, relative blade element thrust
$V$	=	flow velocity
$W$	=	aircraft takeoff weight
$x, y, z$	=	cartesian coordinates, as subscript for direction
$y^+$	=	dimensionless wall distance
$\alpha, \alpha_{loc}$	=	angle of attack, local flow angle
$\alpha_e$	=	effective angle of attack at blade element
$\beta_{75}$	=	propeller blade pitch angle (at 75 % radius)
$\eta_P, \eta_{Pro}$	=	propeller efficiency, propulsive efficiency
$\rho$	=	density
$\theta$	=	climb angle

#### Subscripts

$\infty$	=	free-stream
$inst, isol$	=	installed, isolated (regarding thrust)
$j$	=	jet

#### Abbreviations

$a/c$	=	aircraft
$CFD$	=	computational fluid dynamics
$HTP$	=	horizontal tail plane
$RANS$	=	Reynolds-averaged Navier-Stokes
$STOL$	=	short takeoff and landing

## I. Introduction

EFFICIENT STOL concepts for commercial aircraft are needed to establish point-to-point connections between compact city airports. As a small noise footprint is particularly important for this kind of operation, the maximum climb angle has to be increased in addition to acoustic treatment.

For this reason, active high-lift systems and noise reduction technologies are currently under investigation in a collaborative research center (SFB 880, funded by Deutsche Forschungsgemeinschaft DFG). Using preliminary design methods, an efficient STOL aircraft for 100 passengers was developed within the framework of this research center at Technische Universität Braunschweig. Core element is a high-lift system with internally blown flaps at the trailing edge. The reference version is a high wing aircraft with two turboprop engines mounted in tractor configuration below the airfoil, see Fig. 1. Several components and related technologies are optimized in the project to develop an advanced version of the airplane.

A major objective of the present study is to enhance the maximum climb angle without increasing thrust-to-weight ratio or wing area. Considering multidisciplinary aircraft design, high engine power and small wing loading have a negative impact on direct operating costs as shown for a similar concept<sup>1</sup>. Looking at the climb angle definition<sup>2</sup>

$$\sin \theta = \frac{T}{W} - \frac{1}{L/D}$$

it is obvious that the lift-to-drag has to be improved. In addition, the thrust-to-weight ratio can be raised without installing more engine power by enhancing the propulsive efficiency  $\eta_{Pro}$ . It is assumed that new propeller integration concepts are necessary to exploit the potentials of  $L/D$  and  $\eta_{Pro}$ . For this reason, two

types of over-the-wing propeller configurations are investigated concerning takeoff performance. Although the effect of such propeller installations on thrust and drag has already been studied in the 1920s<sup>3,4</sup> as well as in the 1980s<sup>5</sup>, only little information is available about the influence of engine integration on high-lift aerodynamics in general and on blown flap systems in particular.

One of the presented configurations, featuring a partially embedded open rotor, was inspired by the *Custer Channel Wing*<sup>6,7</sup>. A comparable channel wing was recently tested in combination with active high-lift to reach extreme lift coefficients<sup>8</sup>. While the propeller is installed near the wing trailing edge in these designs, it is positioned near mid-chord here to furthermore allow for shielding of the propeller noise. Shielding is considered as one of the most efficient measures to reduce ground noise as the propulsion system is a dominant noise source at takeoff.

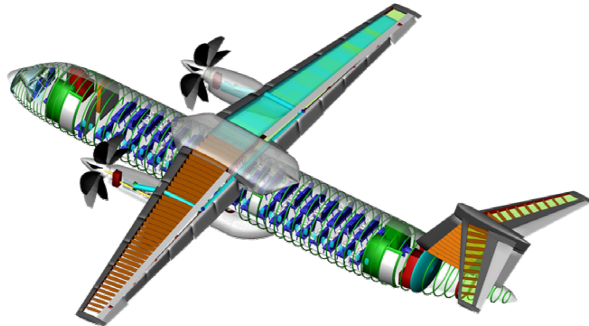


Figure 1. Overview of the reference STOL aircraft from the preliminary design tool PRADO<sup>9</sup>.

## II. Test Case

Only takeoff conditions were considered in this paper in order to focus on the short takeoff aspect of the underlying STOL design. In particular, the point at the very end of the takeoff process was selected where the airplane is 35 ft above the takeoff surface (cf. FAA FAR § 25.113). At a corresponding Mach number of  $Ma_\infty = 0.172$ , preliminary studies found an overall lift coefficient of  $C_L = 2.79$  and a required aircraft thrust coefficient of  $\hat{C}_T = 0.78$  for the reference version. In the wing section where the propeller axis is located, the local lift coefficient is slightly higher with  $c_l = 3.0$  at a Reynolds number of  $Re_\infty = 17 \cdot 10^6$ . As  $c_l = 3.0$  is achieved for the present airfoil (see section A) at  $\alpha = 0^\circ$ , all simulations have been conducted at this single angle of attack.

### A. Wing and Airfoil Geometry

For this basic research work a simplified geometric model was used. In order to exclude aspect ratio dependencies and tip vortices, a symmetry condition was applied at both ends. Based on the reference aircraft, a generic test case with an unswept, rectangular wing ( $l = 3.8$  m,  $b = 5 l$ ) and a propeller with generic nacelle was designed. In coherence with research results at Technische Universität Braunschweig<sup>10,11</sup>, the transonic DLR F15 airfoil<sup>12</sup> geometry was modified by adding a  $0.25 l$  long plain flap with a Coanda type boundary layer control (BLC). In particular, the flow control system consists of a constant-radius Coanda surface and a tangential jet nozzle located upstream. A relative slot height of  $h/l = 0.0625\%$  was found to be optimal in terms of  $\Delta c_{l,max}/\Delta c_\mu$  as a figure of merit. Due to a high blowing efficiency, a jet momentum of only

$$c_\mu = \frac{V_j \cdot \dot{m}_j}{q_\infty S} = 0.03 \quad (1)$$

is needed for the flap angle of 45 degrees to ensure attached flow<sup>10</sup>.

### B. Propulsion Unit

With the required static thrust known from the preliminary aircraft design, an existing propeller<sup>13</sup> which was originally designed for a related STOL research project (*Bürgernahe Flugzeug / Citizen-Friendly Aircraft*)<sup>14</sup> was adapted to the present requirements. Hence, its diameter was reduced from  $D_P = 6$  m to

$D_P = 5$  m while increasing the shaft speed to keep the blade tip Mach number of  $Ma_{tip} = 0.7$ . The intention was to therefore maintain aerodynamic and acoustic characteristics concerning efficiency and low noise levels, respectively. With nine highly loaded blades, the rotor of this constant speed propeller is similar to propfan designs. The blade geometry is the result of a two-point design, aiming at high takeoff thrust at low rotational speed and high efficiency in cruise flight.

### C. Configurations

A total of four simplified configurations have been investigated to allow for a reasonable comparison between the fundamental types of engine integration, see Fig. 2. Besides a conventional tractor configuration, two different types of over-the-wing mounted propellers have been considered. Among these is a channel wing type configuration where the rotor is embedded into the wing. In contrast to the Custer Channel Wing, the depth of the channel was reduced to one third of the propeller radius and a constant gap between blade tip

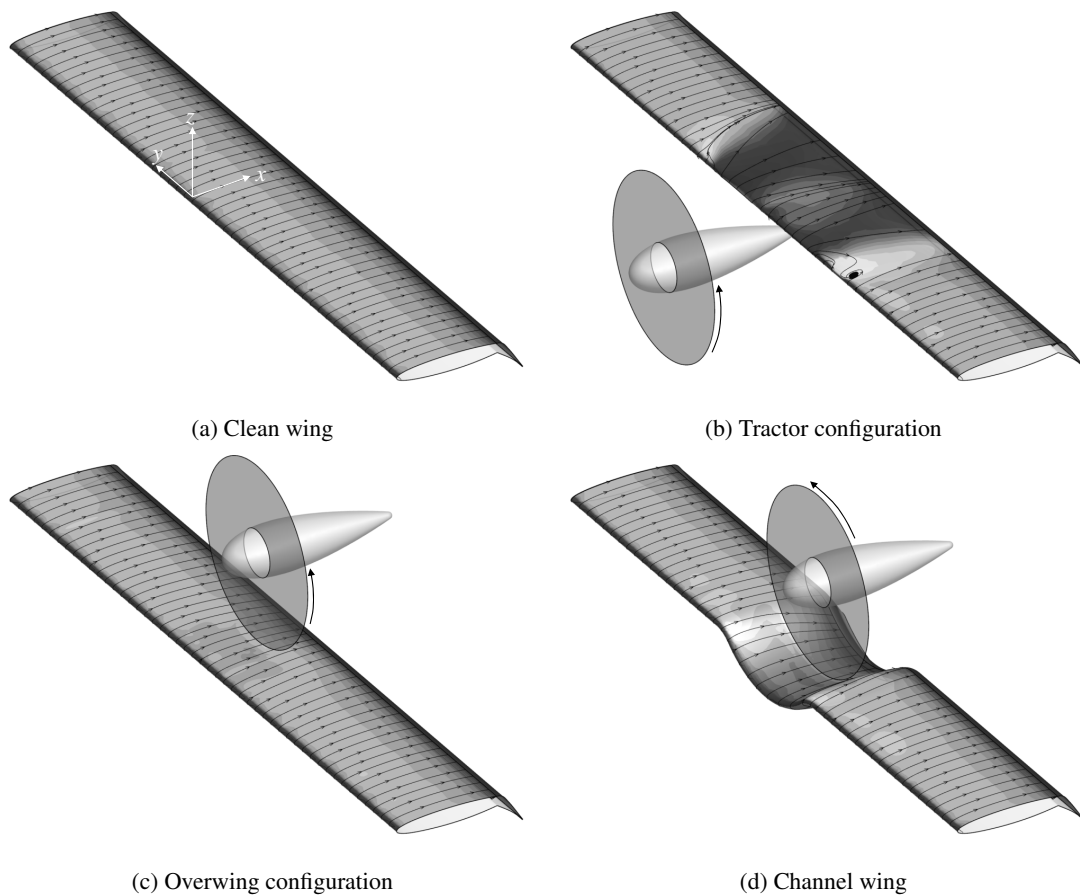


**Figure 2. Geometry of the simulated configurations with added surface streamlines and skin friction coefficient distribution. Large  $c_f$ -values indicated by dark grey.**

and wing surface of  $d/D_P = 0.01$  was chosen. As indicated by Fig. 2, a radius was applied on the junction between channel and outer wing in order to avoid crossflow-induced separation as well as self-intersection problems of the deflected flap.

### III. Numerical Setup

#### A. Computational Domain and Grid

As shown in Fig. 3, the wing segment was incorporated into a cylindrical farfield with a radius of ten chord lengths. All wing and nacelle surfaces were assigned a turbulent viscous wall condition. The unstructured grid (Slot detail on side wall shown in Fig. 4) was created by the commercial grid generator *Centaursoft Centaur* and contained approx. 25 Mio. cells for the 3D test cases. As part of preliminary 2D simulations, grid sensitivity studies with three different sizes were performed to reveal discretisation error dependencies. Hence, a reasonable grid size was determined while the dimensionless wall distance of the first cell does not considerably exceed  $y^+ = 1$ . In order to further improve the accuracy of the 3D solution, regions of expected high gradients like propeller slipstream and wake were refined by means of grid sources, see Fig. 5.

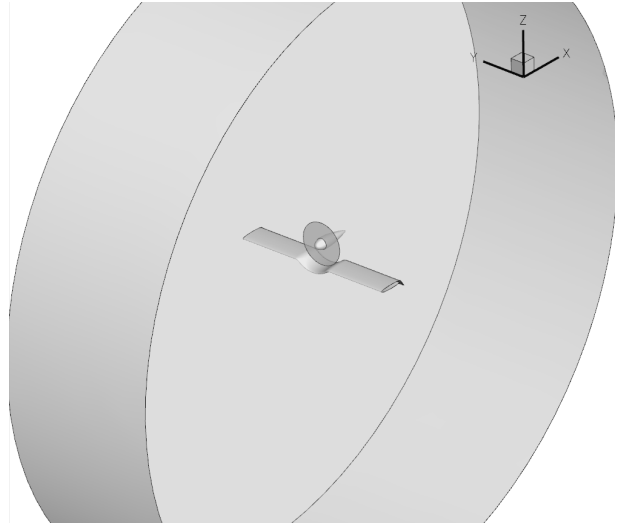


Figure 3. Computational domain geometry.

#### B. Numerical Method

The steady CFD simulations were conducted by using the *DLR TAU code* for solving the RANS equations on the unstructured grids. Turbulence was modeled by the Spalart-Allmaras one-equation formulation<sup>15</sup> with a correction for rotational flow<sup>16</sup>. While the inviscid fluxes of the Navier Stokes Equations were discretized by a central scheme with scalar dissipation, the 2nd order upwind scheme by Roe was used for the convective fluxes of the turbulence equations. On the other hand, all viscous fluxes were discretized by a central scheme using a full gradient approach. A backward Euler relaxation solver was chosen to enable an implicit time integration scheme. The influence of laminar boundary layers on the aerodynamic properties was assumed to be negligibly small at  $Re = 17 \cdot 10^6$  so that all solid surfaces were treated fully turbulent.

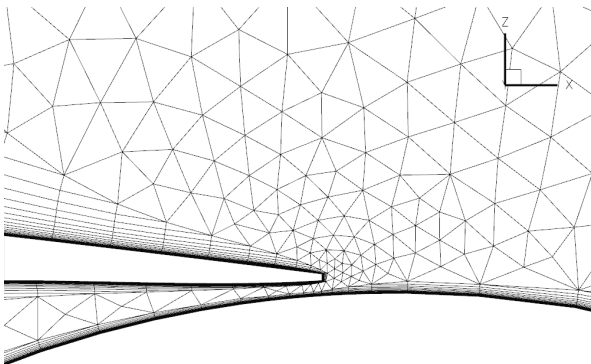


Figure 4. Slot detail of surface mesh on the side wall.

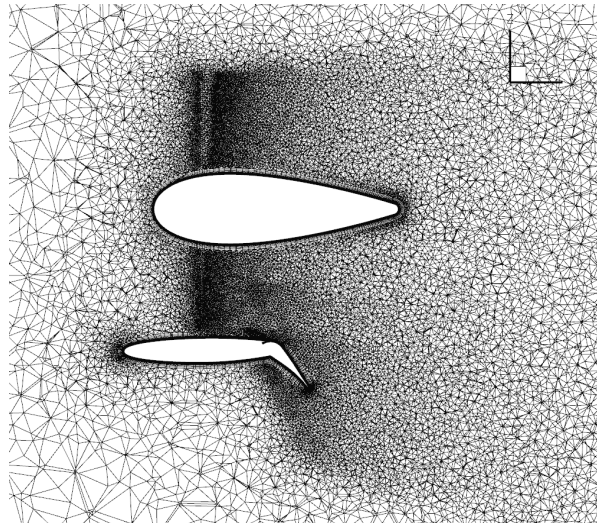


Figure 5. Cross section view of 3D mesh at  $y = 0$ .

### C. Actuator Disc

In order to save computation time, the propeller was modeled by a reactive actuator disc<sup>17</sup>, see Figs. 6 and 7. This means that the inhomogeneous inflow of an installed propeller is taken into account as the variable disc forces are computed through blade element theory. According to the propeller design, the distribution of blade twist and chord length as well as the aerodynamic characteristics at discrete radii were prescribed. In practice, lift and drag over  $\alpha$  was defined for five blade profile sections and a reasonable range including stall behavior. The number of blades, rotational speed and pitch angle had to be specified as well.

From a potential theory point of view, the zero-thickness disc acts like a singularity that applies stationary forces to the fluid, leading to a jump in total and static pressure. As a consequence, flow accelerates smoothly up- and downstream of the actuator similar to a fully simulated propeller. Circumferential forces lead to a realistic swirl in the propeller slipstream while, however, only quasi steady effects can be captured.

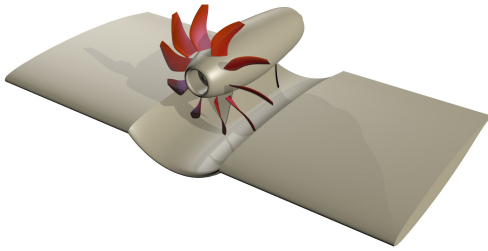


Figure 6. Impression of full propeller and channel wing geometry.

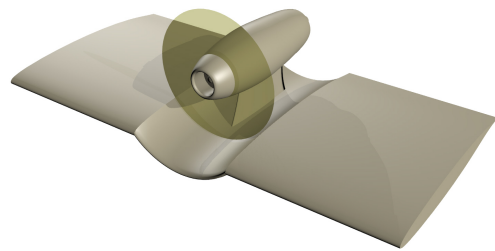


Figure 7. Application of an actuator disc model.

## IV. Results

### A. Influence of the Wing on the Propeller

Although the influence of the open rotor on the wing flow is more obvious, the reverse effect cannot be neglected when aiming at a close coupling. Using the blade element theory model for the actuator disc, local flow conditions such as flow angle and velocity have been taken into account. Fig. 8 shows the undisturbed flow field around a wing section with internally blown flap where two possible propeller installations are indicated by vertical lines. A propeller in tractor position forward of the wing operates at a significant local flow angle  $5^\circ < \alpha_{loc} < 10^\circ$  which is larger than the angle of attack  $\alpha = 0^\circ$  due to the strong upwash of the high-lift wing. On the other hand the local flow direction at the over-wing position is nearly horizontal while the propeller has to operate in a strong vertical gradient of inflow velocity.

Although the propeller itself increases and partially equalizes the local axial velocity level, the wing-induced inhomogeneity has a heavy impact on the effective blade angle of attack, thus blade loadings, see Fig. 9. While a blade element of an isolated pro-

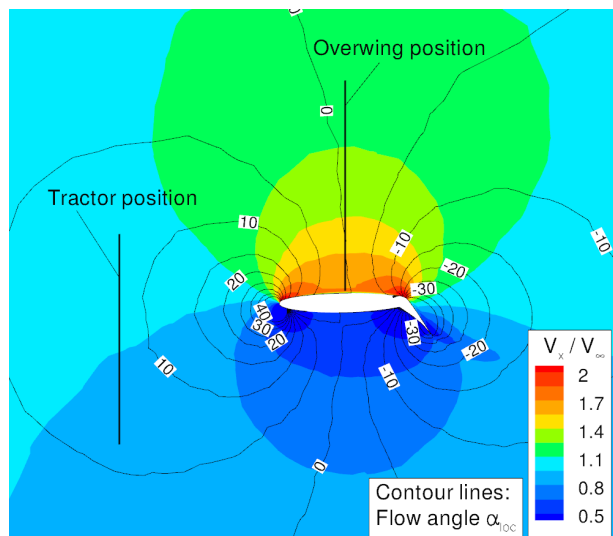
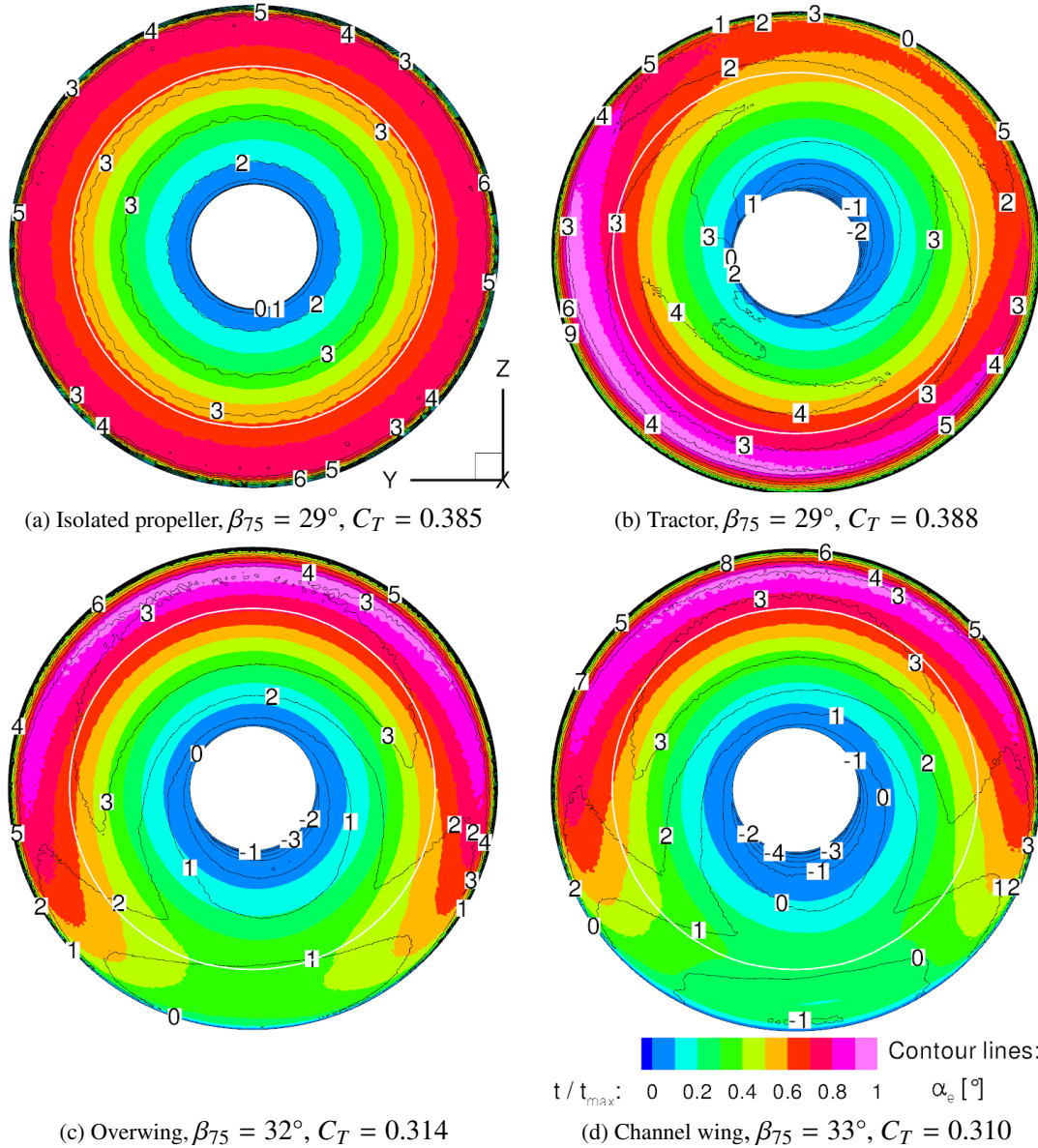


Figure 8. Possible propeller locations in the undisturbed flow field of a high-lift airfoil.



**Figure 9.** Distributions of (effective) blade angle of attack  $\alpha_e$  and relative local thrust  $t/t_{max}$  at  $\alpha = 0^\circ$  and  $C_{P,S} = const. = 0.457$ . The white circle indicates the radius where  $\beta_{75}$  is applied.

propeller produces constant thrust during its revolution depending on the designed blade circulation profile (Fig. 9 (a)), this is not true anymore in an inhomogeneous environment. One effect observed only for the tractor propeller in Fig. 9 (b) is the horizontal shift in load due to the inflow angle ahead of the wing. In contrast, the overwing types suffer from a considerably higher vertical gradient. Even with increased blade pitch angle ( $\Delta\beta_{75} = 4^\circ$ ) to maintain the shaft power of the isolated rotor, only very little thrust is generated in proximity to the wing surface. Hence, the overwing and channelwing propellers lose 19 % and 20 % of the net thrust, respectively, and thus an equal amount of propeller efficiency

$$\eta_P = \frac{T \cdot V_\infty}{P_S} \quad (2)$$

at the same shaft power coefficient

$$C_{P,s} = \frac{P_S}{\rho_\infty \cdot D_P^5 \cdot n^3} \quad (3)$$

A reasonable solution is the adaption of  $\alpha_e$  through pitch, twist, and shaft axis orientation. The propeller-related measures are discussed in section V.

## B. Influence of the Propeller on the Wing

### 1. Flow Field at Midspan Cross Section

By simulating infinite span, two-dimensional flow occurs around the clean wing. Streamlines and Mach number distribution (Fig. 10 (a)) reflect the proper usage of the Coanda effect where the flow along the 45°-flap stays attached by wall jet blowing with  $c_\mu = 0.03$ . The resulting flow field indicates strong circulation and high velocities at the nose and Coanda surface. Adding a propeller in tractor configuration and applying takeoff thrust, the flow around the high-lift wing is significantly changed, see Fig. 10 (b). The slipstream shows an increased velocity ( $\Delta Ma \approx 0.1 \dots 0.2$ ) and gets redirected by the blown flap. This kind of thrust vectoring can generate a large proportion of lift gain on takeoff configurations as also observed for the Custer Channel Wing<sup>8</sup>. However, the moderately embedded propeller of the investigated configuration does not show significant thrust vectoring (cf. Fig. 10 (d)), at least for  $\alpha = 0^\circ$ . Looking at Fig. 10 (c), it is striking that the lower surface flow is nearly unchanged by engine integration when positioning the actuator disc above the midchord of the wing.

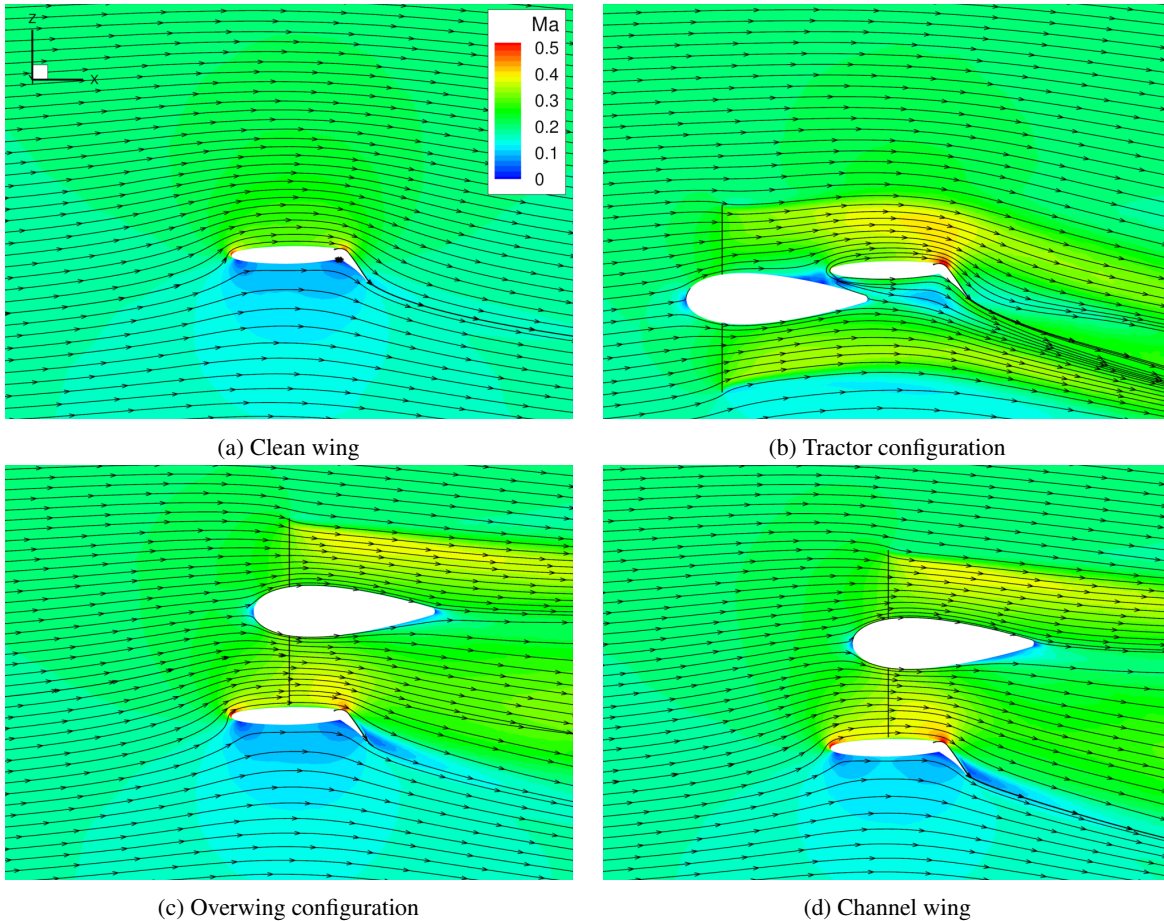


Figure 10. Streamlines and Mach number distribution at  $y = 0$ .

## 2. Pressure Distributions and Surface Flow Pattern

Considering the tractor configuration in terms of the midspan ( $y = 0$ ) pressure distribution (Fig. 11), the massive suction peak on the Coanda surface reflects the slipstream deflection observed in Fig. 10 (b). Together with a high pressure area on the lower surface close to the flap hinge, the major part of additional lift (compared to the clean wing) is generated on the rear part of the wing. Different mechanisms are found for the overwing configurations. While the whole static pressure level on the upper surface is amplified by the higher momentum in the slipstream, the lower surface shows the same distribution as a clean wing. However, the suction force of the tractor configuration cannot be achieved as the static pressure increases rapidly in the propeller disc plane, cf. Fig. 11. The dominating, long suction peak therefore leads to a more front loaded pressure distribution with a potential to reduce the nose-down pitching moment which is an issue for such high-lift configurations.

Further significant differences between the two fundamental propeller configurations can be identified when looking at the three-dimensional surface flow. Going back to Fig. 2 (b), wall streamlines and skin friction distribution (grey shades) indicate a diverging, high-friction flow pattern on the upper wing surface which is located in the slipstream region of the tractor propeller. Asymmetric features like the small separation vortex near the leading edge are most likely due to a swirl-induced up- and downwash distribution along the span. As this effect does not exist for both overwing configurations, near-wall flow appears almost symmetric. In contrast to the conventional tractor design, the friction level is much lower on the channel wing surface and the wall streamlines tend to converge. Judging on wing surface flow, interaction is very small for a plain overwing configuration (compare Fig. 2 (a) and Fig. 2 (c)).

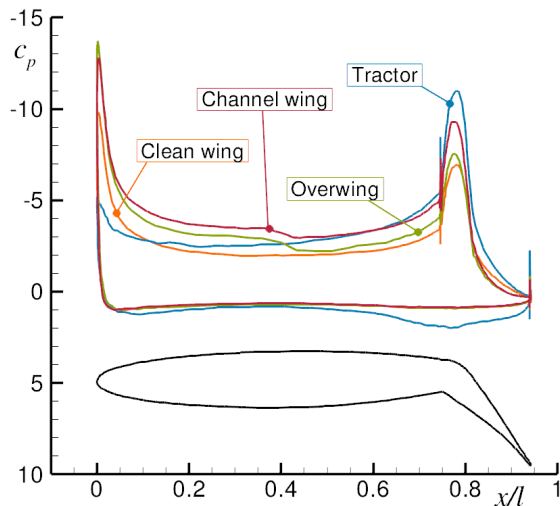


Figure 11. Pressure distributions at  $y = 0$ .

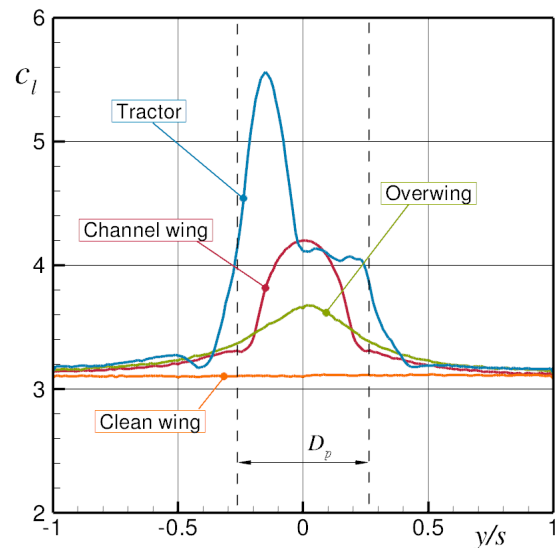


Figure 12. Spanwise distribution of lift coefficient.

## 3. Aerodynamic Coefficients

Relevant information concerning aerodynamic performance can be extracted from the spanwise distribution of lift, drag and pitching moment coefficients, see Figs. 12-14. As indicated by the pressure distributions, lift increases in the area blown by the propeller slipstream with a maximum near midspan. According to the surface flow analysis (section 2), the distribution of the aerodynamic coefficients is highly asymmetric for the tractor configuration where the propeller swirl leads to a spanwise variation in effective angle of attack.

In addition to the high friction drag (note  $c_f$ -distributions), pressure drag is increased by the backward-pointing suction peak on the Coanda surface on the one hand and high pressure in a stagnation area near the flap hinge on the other hand (see Figs. 11 and 13). It should be mentioned that the drag is dominated by pressure drag for this wing - especially in the propeller section. In contrast, both over-the-wing propeller configurations benefit from the fact that a significant fraction of the additional lift arises from forward-pointing surfaces near the nose. Hence, negative drag or respectively induced thrust can be observed in the corresponding region. For this configuration, the nose-down pitching moment (Fig. 14) is therefore comparable to a clean wing while it reaches very high negative values for the combination of tractor propeller and high-lift wing.

The channel wing as compared to a simple overwing design helps to increase the lift gain by a factor of two while drag and pitching moment are slightly worse. Although the clearance between propeller tip and wing surface is identical at midspan for both versions, a constant gap along a considerable portion of the wingspan is important when aiming at high-lift capabilities.

### C. Assessment of the Overall Configuration

#### 1. Approach

Having the mutual influence between propeller and wing in mind it is clear that both parts of the configuration cannot be assessed separately. For this reason a balance of important forces and moments shall be established for the complete reference aircraft (cf. Fig. 15 (a)). A distinction is made between a high-wing configuration for the tractor propeller and a low-wing configuration for the two overwing propeller designs, see Figs. 15 (b) - (d). With the wing root and tip being fixed, the channel wing propeller and corresponding wing section are located below the ones of a straight wing.

The basis for this investigation is the STOL airplane mentioned in Chapter I, whose aerodynamic surfaces were sized by preliminary design tools neglecting any propeller influence. As this case is represented by the clean wing configuration (Fig. 2 (a)), the installation effects can be estimated by comparison with the simulated propeller configurations. It is assumed that, for example, the propulsion-induced lift increment  $\Delta L$  of the generic wing segment is also valid for the entire aircraft when applying the same Reynolds and Mach numbers. In fact, the dynamic pressure at free-stream is identical while the chord lengths match at

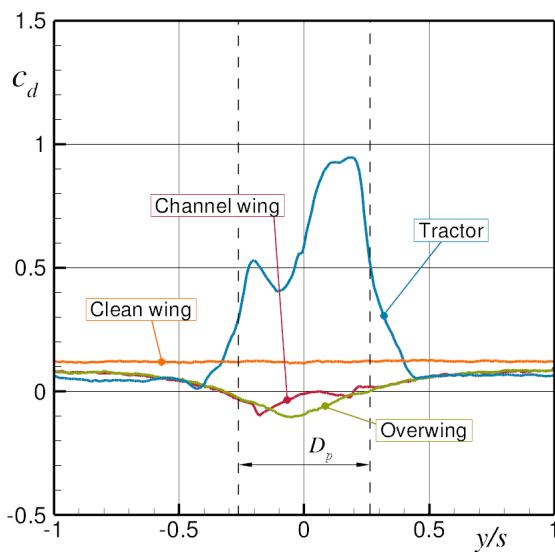


Figure 13. Spanwise distribution of drag coefficient.

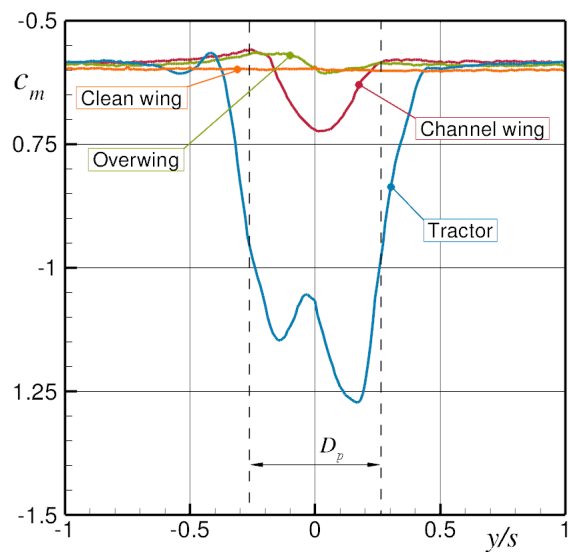
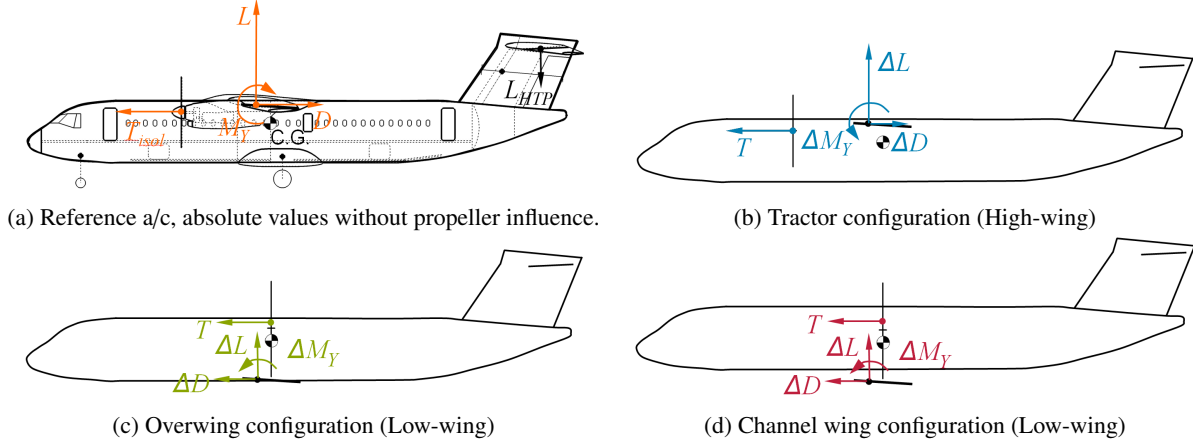


Figure 14. Distribution of pitching moment coefficient.



**Figure 15. Delta forces resp. pitching moment and absolute thrust for balancing the overall configuration.**

the spanwise propeller position. To take the limited wingspan and trapezoidal planform of the actual design into account, only the delta forces on the most affected segment ( $-0.5 < y/s < 0.5$ ) of the rectangular wing were considered. To be precise, the differences in  $c_l$ ,  $c_d$  and  $c_m$  (Figs. 12-14) between clean wing and each propeller configuration were integrated along this part of the span as well as multiplied by  $l$  and  $q_\infty$  to get  $\Delta L$ ,  $\Delta D$  and  $\Delta M_y$ . The resulting values and the thrust  $T$  were subsequently multiplied by the number of engines, two, and normalized with  $q_\infty$ ,  $S_{ref}$  and  $l_{MAC}$  to obtain the delta coefficients relevant for the overall aircraft design.

## 2. Balance of Forces and Figures of Merit

Looking at Table 1, it is striking that one has to pay a high price for generating additional lift  $\Delta C_L$  by a high-lift tractor configuration as the installed thrust coefficient

$$\hat{C}_{T,inst} = \frac{2 \cdot T_{inst}}{q_\infty \cdot S_{ref}} = \hat{C}_T - \Delta C_D, \quad \text{with} \quad \hat{C}_T = \frac{2 \cdot T}{q_\infty \cdot S_{ref}} \quad (4)$$

drops down ( $\Delta \hat{C}_{T,inst} < 0$ ) due to a considerably higher drag coefficient ( $\Delta C_D > 0$ ). Things are completely different for overwing propeller installations where more drag is saved on the wing than thrust is lost on the actuator disc. Hence, 28 % to 32 % more installed thrust is achieved, almost reaching the isolated thrust coefficient  $\hat{C}_{T,isol} = 0.783$ . This behavior is reflected by two figures of merit (FoM), namely the lift-to-drag ratio

$$\frac{L}{D^*} = \frac{C_L}{C_D^*} = \frac{C_{L,ref} + \Delta C_L}{C_{D,ref} + \Delta C_D^*} \quad (5)$$

and propulsive efficiency

$$\eta_{Pro} = \frac{T_{inst} \cdot V_\infty}{P_S} \neq \eta_P. \quad (6)$$

The absolute lift and drag coefficients ( $C_{L,ref}$ ,  $C_{D,ref}$ ) are obtained from preliminary design data of the reference aircraft at takeoff. To allow comparability of the lift-to-drag ratio at different thrust values, the drag increment has been corrected by  $\Delta \hat{C}_T = \hat{C}_T - \hat{C}_{T,isol}$  to get  $\Delta C_D^* = \Delta C_D - \Delta \hat{C}_T$ . Considering this figure, both overwing configurations nearly reach the magnitude  $L/D = 7.32$  of a fully isolated test case without interaction while a tractor configuration performs worse (cf. Table 2). This indifferent channel wing result may be further improved by using the potentials of propeller or blade adaptation such as cyclic pitch.

Moreover, one should not forget the noise shielding capability for this kind of configuration which still has to be explored.

Coefficient	Tractor	Overwing	Channel wing
$\Delta C_L$	0.661	0.241	0.339
$\Delta C_D$	0.2231	-0.1055	-0.0945
$\Delta \hat{C}_T = \hat{C}_T - \hat{C}_{T,isol}$	0.005	-0.145	-0.154
$\Delta \hat{C}_{T,inst} = \hat{C}_{T,inst} - \hat{C}_{T,isol}$	-0.218	-0.039	-0.059

**Table 1. Impact of propeller installation on the lift, drag and thrust coefficients of the a/c.**

FoM	Isolated Wing resp. Propeller	Tractor	Overwing	Channel wing
$L/D$	7.32	5.71	11.00	10.92
$L/D^*$	7.32	5.76	7.21	7.11
$\eta_P$	0.61	0.61	0.50	0.49
$\eta_{Pro}$	0.61	0.44	0.58	0.57

**Table 2. Corrected lift-to-drag ratio and propulsive efficiency as figures of merit for the overall configuration. The lift-to-drag ratio of the wing and the propeller efficiency are given for comparison reason.**

### 3. Balance of the Pitching Moment

The structurally unfavorable integration of a channel into the wing, however, can only be justified when considering pitching moment dependencies, see Table 3. While the additional nose-down pitching moment  $\Delta C_{M,y}$  is a disadvantage for a plain over-the-wing propeller, even a small channel depth of  $D_P/6$  reduces this coefficient by  $\Delta(\Delta C_{M,y}) = 0.14$  when compared to the tractor configuration. For the underlying aircraft geometry a potential of saving 10 % HTP area was found. It shall be mentioned that lift, drag and especially thrust contribute significantly to the total pitching moment when calculated around the center of gravity. The influence of the corresponding lever arms should not be neglected as they are different for all configurations.

Source	Tractor	Overwing	Channel wing
$\Delta C_{M,y}$	-0.2738	0.0126	-0.0126
$\Delta C_L$	0.1132	0.0410	0.0580
$\Delta C_D$	0.0847	0.0780	0.0698
$\hat{C}_T$	-0.1724	-0.4447	-0.2243
Total $\Delta C_{M,y,total}$	-0.2483	-0.3131	-0.1091

**Table 3. Impact of propeller installation on the pitching moment coefficient around the center of gravity of the a/c.**

## V. Conclusions and Outlook

Numerical investigations have been conducted at takeoff conditions for a high-lift wing with internally blown flap. A clean wing, a tractor configuration and two over-the-wing propeller designs were compared at moderate angle of attack ( $\alpha = 0^\circ$ ). It is shown by propeller load distributions and aerodynamic coefficients of the wing that the mutual influence between these two elements is fundamentally dependent on the type of engine integration. An assessment of the overall configuration reveals some important benefits for a channel wing configuration:

- Compared to a tractor, the lift-to-drag ratio  $L/D^*$  and propulsive efficiency  $\eta_{Pro}$  increase by 23 % and 30 %, respectively, almost reaching the level of an isolated wing and propulsion system.
- The overall nose-down pitching moment is much lower than for both tractor and plain overwing configurations, allowing a 10 % smaller HTP area in relation to the reference.
- Wall streamlines appear almost symmetric and parallel which may enable laminar flow regions upstream of the propeller.

Apart from the fact that the simple channel wing design under consideration in this study cannot achieve the lift augmentation of a conventional tractor layout, some disadvantages arise from the inhomogeneous propeller thrust distribution:

- For a constant power coefficient, the net thrust and hence the positive effects on the wing decrease.
- The eccentrically acting thrust force vector contributes to the nose-down pitching moment as well as inducing a bending moment in the shaft.
- Due to cyclic propeller blade forces, vibrations may occur causing structural problems while additional interaction noise is generated.

These drawbacks can be, at least partially, avoided through an adaptive propulsion unit as mentioned before. To give an outlook, three technical solutions are suggested by the authors and will be evaluated in future work:

- Reorientation of the propeller shaft axis, mainly by rotating around the yaw axis. While a constant flow angle is induced on the disc, the resultant angle at the rotating blade element depends on the azimuth. It can therefore increase  $\alpha_e$  in the proximity of the wing. Axial thrust is decreased by the cosine of the rotation angle.
- Applying cyclic pitch by the use of a swashplate. Compared to the above measure, a more constant  $\alpha_e$ -distribution may be achieved for a certain radius. Cyclic variations, albeit weaker, still occur at other radii. The installation of a swashplate and actuation system adds to the cost and complexity of the engine.
- Flexible, actuated blade structure. A cyclic individual twist variation of the propeller blades is able to realize the desired  $\alpha_e$ -distribution independent of the inflow conditions. Although this technology is not yet in operation, it is currently under investigation considering droopnose and helicopter blade applications.

Apart from this, further work will extend the study to cruise condition where thrust effects are much smaller and  $L/D$  is more sensitive to drag. Furthermore, the channel wing geometry shall be adapted on a parametric basis to take the propeller flow into account and thus enhance synergetic effects.

## VI. Acknowledgements

This work was funded by the Deutsche Forschungsgemeinschaft DFG (German Research Funding Organisation) in the framework of the collaborative research center SFB 880. The authors would like to greatly acknowledge Axel Raichle, DLR Braunschweig, Institute of Aerodynamics and Flow Technology for his extensive support regarding the actuator disc model in TAU. Further thanks go to Carsten Lenfers (DLR) for providing propeller data and Nils Beck (TU Braunschweig) and Jochen Wild (DLR) for providing the wing airfoil geometry. We would also like to acknowledge Wolfgang Heinze of the Institute of Aircraft Design and Lightweight Structures, TU Braunschweig for his multidisciplinary studies on the STOL aircraft in SFB 880.

## References

- <sup>1</sup>Werner-Spatz, C., Heinze, W., and Horst, P., "Improved Representation of High-Lift Devices for a Multidisciplinary Conceptual Aircraft Design Process," *AIAA Journal of Aircraft*, Vol.46, No.6, pp.1984-1994, 2009.
- <sup>2</sup>Anderson, J. D., "Aircraft Performance and Design," McGraw-Hill, 1999.
- <sup>3</sup>Prandtl, L., Wieselsberger, C., and Betz, A., "Gegenseitige Beeinflussung von Tragfläche und Schraube," Ergebnisse der Aerodynamischen Versuchsanstalt zu Göttingen, chap. IV, sec. 6, 3rd edition, Oldenbourg, 1925.
- <sup>4</sup>Prandtl, L., "Mutual Influence of Wings and Propeller," extract from The First Report of the Göttingen Aerodynamic Laboratory, chap. IV, sec. 6, *NACA Technical Notes*, No. 74, 1921.
- <sup>5</sup>Johnson, J. L., and White, E. R., "Over-the-Wing Propeller," *U.S. Patent No. 4'629'147*, 1986.
- <sup>6</sup>Pasamanick, J., "Langley Full-Scale-Tunnel Tests of the Custer Channel Wing Airplane," NACA RM L53A09, National Advisory Committee for Aeronautics, April 1953.
- <sup>7</sup>Mitchell, K. A., "Mr. Custer and His Channel Wing Airplanes," *Journal of American Aviation Historical Society*, Spring 1998.
- <sup>8</sup>Englar, R. J. and Campbell, B. A., "Pneumatic Channel Wing Powered-Lift Advanced Super-STOL Aircraft," *Proceedings of the 1st Flow Control Conference 2002*, No. AIAA 2002-3275, St. Louis, MO (USA), 2002.
- <sup>9</sup>Heinze, W., "Private Communication," *Institute of Aircraft Design and Lightweight Structures*, Braunschweig, 2012.
- <sup>10</sup>Jensch, C., Pflingsten, K.-C., Radespiel, R., Schuermann, M., Haupt, M., and Bauss, S., "Design Aspects of a Gapless High-Lift System with Active Blowing", *Proceedings of Deutscher Luft- und Raumfahrtkongress 2009*, Aachen, Germany, 2009.
- <sup>11</sup>Beck, N., Wentrup, M., and Radespiel, R., "Realisierung eines Windkanalexperiments für aktiven Hochauftrieb," *Proceedings of Deutscher Luft- und Raumfahrtkongress 2011*, Bremen, Germany, 2011.
- <sup>12</sup>Wild, J., Wichmann, G., Haucke, F., Peltzer, I., and Scholz, P., "Large scale separation flow control experiments within the German Flow Control Network," *Proceedings of the 47th AIAA Aerospace Sciences Meeting*, Paper No. AIAA 2009-0530, Orlando, FL (USA), 2009.
- <sup>13</sup>Rüdiger, S., Friedrichs, J., and Lenfers, C., "Antrieb und Messtechnik für einen Propeller an einem Windkanalmodell," *Proceedings of Deutscher Luft- und Raumfahrtkongress 2011*, Bremen, Germany, 2011.
- <sup>14</sup>Butzmühlen, C. and Hecker, P., "Das Bürgernahe Flugzeug," *Proceedings of Deutscher Luft- und Raumfahrtkongress 2010*, Hamburg, Germany, 2010.
- <sup>15</sup>Spalart, P. R. and Allmaras, S. R., "A One-Equation Turbulence Model for Aerodynamic Flows," *AIAA Paper*, No. 92-0439, 1992.
- <sup>16</sup>Shur, M. L., Strelets, M., Travin, A. K., and Spalart, P. R., "Turbulence Modeling in Rotating and Curved Channels: Assessing the Spalart-Shur Correction," *AIAA Journal*, Vol. 38, No. 5, pp. 784-792, 2000.
- <sup>17</sup>Raichle, A., Melber-Wilkening, S., and Himisch, J., "A New Actuator Disk Model for the TAU Code and Application to a Sailplane with a Folding Engine," *Proceedings of the 15th STAB/DGLR Symposium*, Darmstadt, Germany, 2006.